GBT MEMO 207

Analysis of cardinal point survey data

Don Wells*

October 16, 2000

Abstract

A least-squares model has been fitted to the data from a survey of retrospheres attached to "cardinal point" nodes of the GBT feedarm and box structure and to the elevation bearings. The LS fit includes gravitational deflections from the as-built finite-element model of the GBT. The azimuth zero point (a traditional pointing model parameter) and the elevation of the elevation axle can be estimated from the data, and the vector offsets of the retrospheres from nearby nodes can be determined. The trajectory of the tip of the feedarm is discussed, including the deflection out of the plane-of-symmetry. The lateral position of the azimuth axis w.r.t. the "ring-of-fire" is estimated from measurements of the four elevation bearing retrospheres.

Contents

*mailto:dwells@nrao.edu

1 The "cardinal point survey" dataset

The "cardinal points" are a set of nodes (truss joints) on the GBT feedarm and box structures which were chosen by L. King [Kin96] because of their importance for understanding and calibrating the gravitational deflections of the structure. All of the cardinal point targets measured in this dataset are *spherical retroreflectors* (also called *retrospheres* or *ball retroreflectors*) which are attached to the structure near the selected nodes. The properties and use of the retrospheres have been described by Goldman [Gol96].

Dave Parker and John Shelton provided [PS00] a file containing ground-reference XYZ locations of retroreflectors on the GBT for various azimuths and elevations, measured with NRAO's Topcon[1] GTS-301 geodetic total station (*not* NRAO's laser rangefinder instruments). The total station produces measurements of range plus two angles, which were converted to the equivalent XYZ coordinates. The extra optical path inside the retrospheres was corrected during the reduction of the total station data, so that the XYZ values which are analyzed here represent the observed positions of the invariant reflection points inside the retrospheres.

The dataset contains one measurement on each of three retroreflectors (ZEG11060, ZEG11460L, ZEG11460R) on the front of the box structure; these were insufficient to solve for geometric parameters associated with these locations, and so they are not discussed further here. The dataset contains three other groupings of targets which will be used in three least-squares solutions:

- A considerable number of measures of five retroreflectors (ZEG20440L[2], ZEG20440R, ZEG21440L, ZEG21440R, ZEG31020, see Figure 1 on the facing page) on the "elbow" of the feedarm, for various elevations at a single azimuth; these are able to support a solution for the elevation axle location and for the locations of these retroreflectors (see Section 2 on page 5, especially Table 3 on page 9).
- Three nodes at the tip of feedarm (ZEG41040L, ZEG41040R, ZEG41080, see Figure 1 on the next page, Figure 2 on page 4 and Figure 3 on page 19) were measured along with the five elbow nodes; these are able to support a solution for their positions and corrections to their gravity deflection terms (see Section 3 on page 13, especially Table 10 on page 13 and Table 14 on page 16).
- The dataset contained XYZ positions of the four retroreflectors mounted under the elevation bearings (ZAG731D, ZAG731P[3], ZAG736D, ZAG736P, see Figure 7 on page 23), for several azimuths; these are able to support a solution for their coordinates in the azimuth coordinate system plus the lateral position of the azimuth axis (see Section 4 on page 23, especially Table 20 on page 24 and Table 25 on page 26).

1.1 The rôle of the Finite Element Model [FEM]

The nodes of the GBT tipping structure are displaced by gravity as the telescope moves in elevation. If these displacements are not compensated they will bias any attempt to fit circular arcs to the trajectories of the targets mounted near those nodes. The displacements of the nodes are predicted by the finite-element model [FEM] of the GBT [Wel00]; the displacements of the targets mounted near the nodes will be similar.[4] Two different GBT structural models are available currently: the design reference model called

[1] See `http://www.topcon.co.jp` and `http://www.topconlaser.com/home.htm` (Topcon Corporation, 75-1 Hasunuma-cho, Itabashi-ku, Tokyo, 174-8580 Japan). The Topcon total station (theodolite plus laser rangefinder) range accuracy is specified as $\pm$(3 mm + 2 ppm) m.s.e., and its horizontal/vertical angular accuracy is specified as $\pm$2 arcsec; in practice range data exhibit RMS around 1 mm.

[2] The "L" suffix of this target name means that it is on the left side of the structure ($x_{\text{tipping}} < 0$); "R" targets are on the right, and no suffix is for retroreflectors on the plane of symmetry. A different notation is used in the structural model software [Wel00], where integer numbers are used rather than character strings; the nodes near ZEG20440L, ZEG20440R, ZEG21440L, ZEG21440R and ZEG31020 are called -20440, 20440, -31440, 21440 and 31020 in the FEM code.

[3] The "P" suffix for the 731/736 target name pairs is for "proximal", meaning *closest* to the azimuth axis, while the "D" suffix is for "distal" (farthrest).

[4] Usually a target can be regarded as being attached to the tip of a rigid rod which is attached to the node; the displacement of the tip will be the displacement of the node plus the motion of the tip relative to the node due to rotation of the node, which

"Model 95b", and the as-built model called "Model 97". The mass distribution in Model 95b was symmetric. The current version of Model 97 is also symmetric. However, the mass distribution of the actual GBT is somewhat asymmetric; in particular, the elevator assembly on the right-hand side of the feedarm causes easily detectable asymmetric deflections in the feedarm, as we will see in Section 3 on page 13.

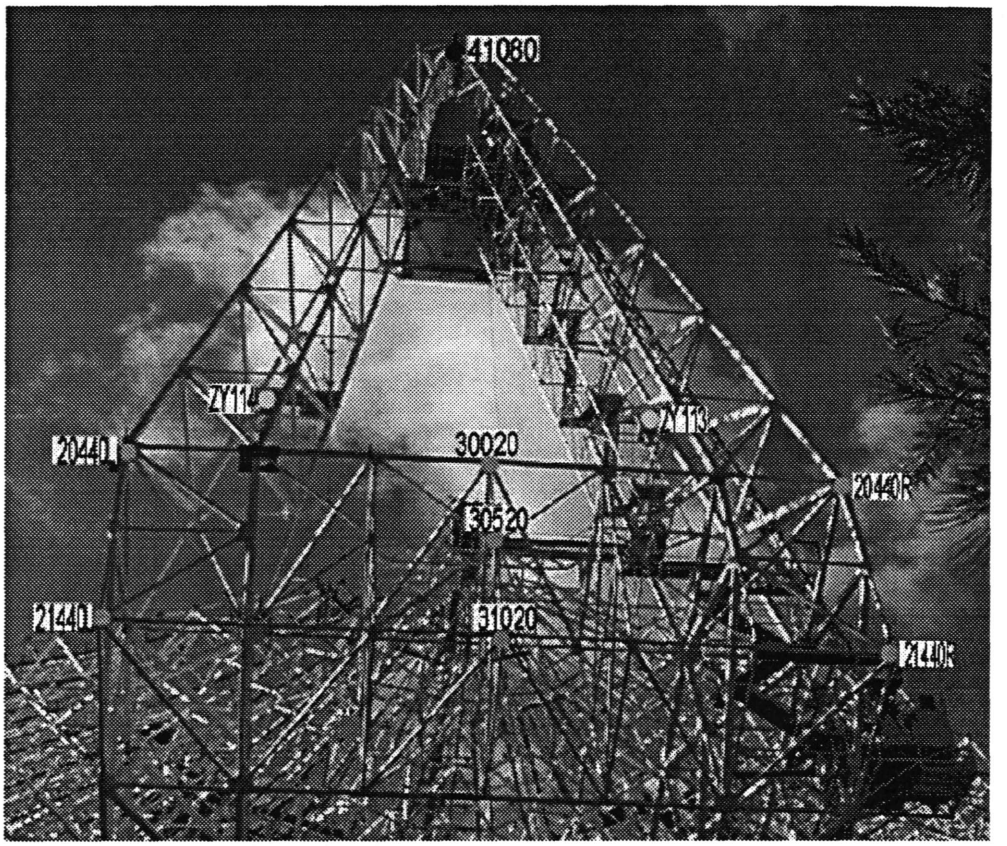

Figure 1: GBT viewed from behind the feedarm, with targets marked

Section 2 on page 5 discusses the fit to the observed trajectories in elevation of five retroreflectors mounted at the "elbow" of the feedarm (labelled 21440L, 31020, 21440R, 20440L and 20440R in Figure 1). The elevation axle position and orientation can be inferred from the five observed arcs, while the coordinate offsets from the nodes to the five targets are also being inferred, with FEM deflections included. If Model 95b is used, the vertical offset of the elevation axle relative to +1900 inches (the nominal design height of the axle above the origin of the coordinate system at the pintle bearing) is estimated to be -47 ± 3 mm, and the inferred lateral offset of the axle (variable **ey** in Table 2 on page 5) is statistically significant, which is physically implausible. However, if the symmetric version of Model 97 is used, the inferred vertical offset (variable **ez**) is -32 ± 2 mm, and the lateral offset is effectively zero. This comparison tells us that the results reported here are sensitive to the choice of FEM. As we will see, even Model 97 does not fully predict the behavior of the structure; therefore we know that the results here must be somewhat biassed. The results reported in the next three sections of this Memo are all based on the version of Model 97 described in Table 1 on the next page:

is also predicted by the FEM. In the present work this rotation is ignored, because it is of order one milliradian, and the targets are less than half a meter from the nodes, so that the extra displacement is only about half a millimeter, which is somewhat less than the precision of the total station measurements.

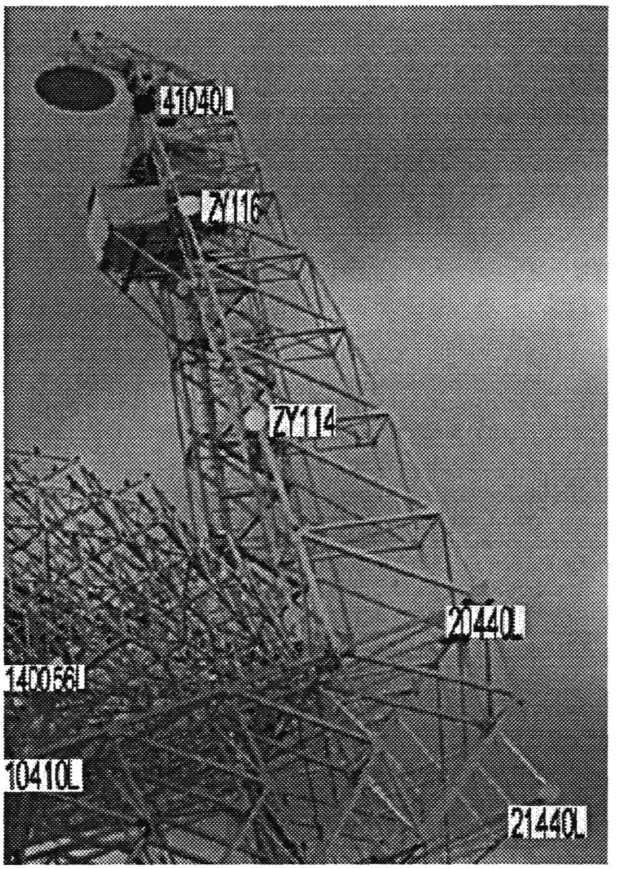

Figure 2: GBT feedarm viewed from the left side, with targets marked

Table 1: Information about the structural model

```
1 fem_filename     = <femA59wM97sG.fef>
  fem_desc         = <Model 97 (L.King symmetric tipping 2000-10-02 [no shrinkage])>
  fem_date         = <Computed Mon 2000-10-02 13:11:41 by ./femComputeFemFile.pl>
  tip_nastran_job = <MSC/NASTRAN JOB CREATED ON 02-OCT-00 AT 11:00:44>
```

The above FEM filename "`femA59wM97sG.fef`" indicates that gravitational deflection ("G") models "59w" of the alidade and "97s" ("s" for symmetric) of the tipping structure are included in the file.

1.2 Geometric parameters measured by surveying

D. Parker [Par00] conducted a separate survey between the GBT elevation axle and various geodetic ground monuments on 2000-09-28. He measured the elevation of the bearings above sea level to be 855.650 meters, which makes the elevation above the alidade track 48.215 meters, or 1898.228 inches. This is -44 mm relative to $+1900$ inches, which can be compared with the -47 mm and -32 mm values reported above. He also measured the azimuth zero point of the elevation axle, and got -541 arcsec. In the next section of this Memo these measurements will be compared with values inferred from the target measurements.

2 Fit1 solution for axle position & grid coordinates

A target moves along an approximately circular arc as the GBT moves in elevation. The arc lies in a plane. If gravitational deflections are negligible, a normal to the plane is parallel to the elevation axle, and the difference between the azimuth of that normal vector and the azimuth indicated by the encoder is the azimuth zero point of the mounting, one of the parameters of the traditional pointing model.[5] The position of the center of the arc can be estimated in the LS fit; this is the elevation of the axle which was discussed in the previous section.

In general, we do not know the tipping structure coordinates of the targets relative to the nodes *a priori*, but must determine them as part of the LS fit. Furthermore, the FEM is somewhat uncertain, as discussed above, and therefore we want to infer empirical corrections to the terms of the FEM for the targets. Experiments with these solutions show that, at least for the present dataset, the FEM corrections are highly correlated with the solutions for the axle position. Furthermore, the trajectories of the targets near the tip of the feedarm deviate signficantly from circular arcs. Therefore, we will solve for the axle parameters using only the retroreflectors on the 'elbow' of the feedarm, and then lock the axle solution and produce the trajectory of the feedarm tip and the FEM corrections in a second solution. The five elbow targets are near nodes 31020, 20440L, 20440R, 21440L and 21440R, whose locations on the feedarm are shown in Figure 1 on page 3 and in Figure 2 on the facing page.

2.1 The LS model for trajectories as a function of Az & El

Table 2 is a listing of the Gaussfit [JFMM88] model which is used for all three LS fits in this Memo. It contains a function `tipnode2gnd()`, beginning at approximately line 100, which computes the XYZ ground coordinates of a retrosphere target as a function of azimuth and elevation plus a set of parameters. The goal of Gaussfit is to adjust the parameters until the computed and observed XYZ coordinates agree. The parameters for Fit1 are `azc` (azimuth zero correction) declared at line 43 and `dgrid[retro,axis]` declared at line 48. If `ez` (Z offset of elevation axle) were declared as `parameter` at line 42, instead of `constant`, Gaussfit would solve for it too. However, for this Memo, the author chooses to accept Parker's determination, `ez` = −44 mm, which is discussed above, and so this parameter is locked. This discussion of the features of the model continues on page 9, after Table 2:

Table 2: Model for cardinal point survey data

```
1  /* cpsFit1Model.gf --- fit cardinal point survey data
      2000-09-15: D.Wells, NRAO-CV
      2000-09-27: add locking of grid offsets when Fit2
      2000-10-10: lock coord diffs of 'ZAG' retrosphere pairs when Fit3
5  */
                    [GNU General Public License copyright notice omitted;
                       see http://www.gnu.org/copyleft/gpl.html]
```

continued on next page

[5] In general, the normal vector will not be horizontal, because the azimuth track is not generally exactly horizontal and because the elevation axle is not generally parallel to the mean plane of the track. The deviation of the track from horizontal has two components, a tilt in the east-west direction and a tilt in the north-south direction. These can be measured by determining the deviation of the vector normal to the track from the gravity vector, and then correcting for the local deviation of gravity from the geodetic vertical (of order 3 arcsec at GB: see `DEFLEC99` at `http://www.ngs.noaa.gov/GEOID/models.html`). These zenith vector components are two of the terms of the traditional pointing model [Con92, Wel98a]. The difference of the axle vector from the plane of the track is the horizontal collimation error of the elevation axle, another one of the terms of the traditional pointing model. In the present Memo we will not determine these three pointing model terms, because we have insufficient data for different azimuths. However, the Gaussfit model in Table 2 already defines the three parameters (`eac`, `zvy`, `zvx`) at lines 39–45 and applies them with statements at lines 132–133 and 156–158, and so we are ready to solve for these pointing model terms when suitable metrology data are acquired.

continued from previous page

Model for cardinal point survey data

```
constant    rig,                  /* [deg] GBT rigging angle              */
            convang,              /* [deg] 'convergence angle' of azimuth*/
            grid[retro,axis],     /* [mm]  design coords node near retro */
            csystem[retro],       /* []    1=tipping coors, 0=alidade     */
            ztrans[retro,axis],   /* [mm]  zenith  gravity transl node    */
            htrans[retro,axis];   /* [mm]  horizon gravity transl node    */
constant    zag, r731p, r731d,    /* []    elev bearing retro flag,       */
            r736p, r736d;         /*       'retro' codes for 4 sph retros */

constant    eac;                  /* [arcsec] elevation axle collimation */
constant    ex;                   /* [mm]  X offset of elevation axle    */
constant    ey;                   /* [mm]  Y offset of elevation axle    */
constant    ez;                   /* [mm]  Z offset of elevation axle    */
parameter   azc;                  /* [arcsec] az zero point correction   */
constant    zvy;                  /* [arcsec] zenith vector east [aboutY]*/
constant    zvx;                  /* [arcsec] zenith vector north[aboutX]*/
constant    px;                   /* [mm]  X coord of pintle bearing     */
constant    py;                   /* [mm]  Y coord of pintle bearing     */
constant    pz;                   /* [mm]  Z coord of pintle bearing     */

parameter   dgrid[retro,axis];    /* [mm]  empirical node->retro offset  */
constant    dlock[retro,axis];    /* [mm]  nonzero is dgrid[,] constraint*/
constant    dztrans[retro,axis]; /* [mm]  retro zenith  gravity delta   */
constant    dhtrans[retro,axis]; /* [mm]  retro horizon gravity delta   */

data        retro,                /* []    id number of target           */
            run,                  /* []    'run' number                  */
            az,                   /* [deg] encoder azimuth               */
            el;                   /* [deg] encoder elevation             */
observation x, y, z;              /* [mm]  observed coords of retro      */

main() {
    variable observed[3], computed[3], locked[30,3], i, j;

    for (i = 0; i < 30; i=i+1)
        for (j = 0; j < 3; j=j+1)
            locked[i,j] = 0;

    while (import()) {
        observed[0] = x;
        observed[1] = y;
        observed[2] = z;
        tipnode2gnd(retro, csystem[retro], az, el, computed);
        for (j = 0; j < 3; j=j+1) {
            export(observed[j] - computed[j]);

            /* if Fit2, constrain dgrid[,] values from Fit1: */
            if ((dlock[retro,j] != 0.0) &&
                (locked[retro,j] == 0)) {
                exportconstraint(dgrid[retro,j] - dlock[retro,j]);
                locked[retro,j] = 1;
```

continued on next page

continued from previous page Model for cardinal point survey data

```
            }
        }
    }
    /* Constrain coord diffs for the pairs of 'ZAG' spherical retros: */
    if (zag != 0) {
       exportconstraint(((grid[r736d,0]+dgrid[r736d,0]) -
                         (grid[r736p,0]+dgrid[r736p,0])) - 317.627);
       exportconstraint(((grid[r731p,0]+dgrid[r731p,0]) -
                         (grid[r731d,0]+dgrid[r731d,0])) - 317.525);
       exportconstraint(((grid[r736d,1]+dgrid[r736d,1]) -
                         (grid[r736p,1]+dgrid[r736p,1])) - 0.0);
       exportconstraint(((grid[r731p,1]+dgrid[r731p,1]) -
                         (grid[r731d,1]+dgrid[r731d,1])) - 0.0);
       exportconstraint(((grid[r736d,2]+dgrid[r736d,2]) -
                         (grid[r736p,2]+dgrid[r736p,2])) - 0.0);
       exportconstraint(((grid[r731p,2]+dgrid[r731p,2]) -
                         (grid[r731d,2]+dgrid[r731d,2])) - 0.0);
    }
}

/* Function to compute ground coords of node 'id' at az/el: */
tipnode2gnd(id, csystem, az, elev, xyz) {
    variable i, Deg=0.017453293,
             sin_rig, cos_rig, sin_elev, cos_elev, wt_zen, wt_hor;

    /* Retroreflector 'id' is near FEM node 'id', whose coordinates
       are in grid[,]; dgrid[,] is the offset from node to retro: */
    for (i = 0; i < 3; i=i+1) {
        xyz[i] = (grid[id,i] + dgrid[id,i]);
    }

    if (csystem == 1) {
       /* Node 'id' is part of tipping structure, so xyz[] are the
          undeflected tipping coordinates of the retro; we will need
          to transform xyz[] to alidade coordinates. First we add the
          gravity deflection at the observed elevation: */
       sin_rig = sin(rig*Deg);
       cos_rig = cos(rig*Deg);
       sin_elev = sin(elev*Deg);
       cos_elev = cos(elev*Deg);
       wt_zen = (sin_elev - sin_rig);
       wt_hor = (cos_elev - cos_rig);
       for (i = 0; i < 3; i=i+1) {
           xyz[i] = xyz[i] +
           wt_zen * (ztrans[id,i] + dztrans[id,i]) +
           wt_hor * (htrans[id,i] + dhtrans[id,i]);
       }

       /* Now rotate the deflected node coords in elevation: */
       about_x(xyz, (90 - elev)*Deg);
```

continued on next page

continued from previous page Model for cardinal point survey data

```
        /* And correct for elevation axle collimation error: */
        about_y(xyz, (eac/3600.)*Deg);

        /* Finally translate to height of axle above pintle bearing: */
        xyz[0] = xyz[0] + ex;
        xyz[1] = xyz[1] + ey;
        xyz[2] = xyz[2] + ez + (1900.0*25.4);

    } else {
        /* Node 'id' is part of the alidade structure, so xyz[] are the
           alidade coordinates of the retro; we will add the gravity
           deflection of the alidade node due to the 5000_ton tipping
           structure which is supported by the elevation bearings: */
        for (i = 0; i < 3; i=i+1) {
            xyz[i] = xyz[i] + ztrans[id,i];
        }
    }

    /* The xyz[] coordinates are in azimuth system, so we must rotate the
       (deflected and translated) coordinates in azimuth. 'convang' is the
       'convergence' correction from state plane coordinates to geodetic
       coordinates, and 'azc' is the azimuth encoder zero point: */
    about_z(xyz, ((az - convang + azc/3600.)*Deg));

    /* Correct the rotated azimuth coordinates for the zenith vector: */
    about_y(xyz, (zvy/3600.)*Deg); /* East  component about Y */
    about_x(xyz, (zvx/3600.)*Deg); /* North component about X */

    /* Finally, add the coordinate offsets of the pintle bearing relative
       to the origin of the coordinates of the 'ring of fire' Kelvin
       mounts: */
    xyz[0] = xyz[0] + px;
    xyz[1] = xyz[1] + py;
    xyz[2] = xyz[2] + pz + 807435.0;
}

about_x(v, a) { variable temp;
    temp = +v[1]*cos(a) +v[2]*sin(a);
    v[2] = -v[1]*sin(a) +v[2]*cos(a);
    v[1] = temp;
}
about_y(v, a) { variable temp;
    temp = +v[0]*cos(a) +v[2]*sin(a);
    v[2] = -v[0]*sin(a) +v[2]*cos(a);
    v[0] = temp;
}
about_z(v, a) { variable temp;
    temp = +v[0]*cos(a) +v[1]*sin(a);
    v[1] = -v[0]*sin(a) +v[1]*cos(a);
    v[0] = temp;
}
```

The model specifies the independent variables of the observations (`retro`, `run`[6], `az`, `el`) with the `data` declaration at line 55, and the dependent variables (`x`, `y`, `z`) with the `observation` declaration at line 59. The `while(import())` loop at line 68 reads the independent and dependent variables of each observation in succession. The differences between the computed and observed XYZ coordinates are arguments to the `export()` function, which forms the equations of condition of the LS solution; Gaussfit's goal is to minimize the sum of the squares of these differences.

Several calls to Gaussfit function `exportconstraint()` appear between lines 76 and 98; these are used in Fit2 (Section 3 on page 13) and Fit3 (Section 4 on page 23), and are not active in Fit1.

2.2 Results produced by the first LS solution

The input data file, which was supplied by D. Parker, was filtered with a Perl [WCS96] program, which selected observations of a list of targets specified in a file for each LS fitting problem. The data table for the first fit is shown in Table 3:

Table 3: Survey data, with residuals from model fit

cpsFit1Data										
retro	node	run	x mm	y mm	z mm	az deg	el deg	Δ_x mm	Δ_y mm	Δ_z mm
1	-20440	1	12056	65376	850195	172	95	1	-9	2
1	-20440	1	12168	64651	866621	172	80	-0	-10	3
1	-20440	1	12946	59751	882295	172	65	0	-7	2
1	-20440	1	14337	51004	896154	172	50	0	-5	5
1	-20440	1	16245	39013	907244	172	35	2	3	8
1	-20440	1	18540	24593	914806	172	20	2	11	10
1	-20440	1	21063	8732	918327	172	5	1	17	18
1	-20440	2	18539	24593	914804	172	20	1	10	9
1	-20440	2	16241	39013	907239	172	35	-3	2	3
1	-20440	2	14337	51005	896153	172	50	0	-4	3
1	-20440	2	12947	59753	882292	172	65	1	-5	-0
1	-20440	2	12166	64649	866618	172	80	-2	-12	-1
1	-20440	2	12055	65373	850194	172	95	-1	-12	-0
2	20440	3	-31789	58409	850160	172	95	1	-6	-6
2	20440	3	-31676	57693	866594	172	80	-2	-6	1
2	20440	3	-30891	52799	882272	172	65	2	-4	0
2	20440	3	-29499	44056	896137	172	50	1	-3	3
2	20440	3	-27590	32063	907234	172	35	0	-1	6
2	20440	3	-25294	17638	914801	172	20	-0	0	7
2	20440	3	-22766	1772	918326	172	5	1	2	11
2	20440	4	-31790	58407	850159	172	95	0	-8	-7
3	31020	5	-9891	62122	849435	172	80	5	-4	-1
3	31020	5	-9807	61586	865949	172	65	4	-6	1
3	31020	5	-9050	56841	881763	172	50	5	-5	1
3	31020	5	-7682	48210	895792	172	35	-0	-3	2
3	31020	5	-5791	36286	907082	172	20	-7	5	7
3	31020	5	-3496	21878	914846	172	5	-5	8	5
4	-21440	5	12205	61834	833363	172	95	3	-3	-4

continued..

[6]The numerical code variable run specifies subsets of the observations, which were made at different times; the original data file supplied by D. Parker specified these subsets with alphabetic codes. run is not used in the LS fits described in this Memo, but could be used to model time-variable effects.

continued..

retro	node	run	x mm	y mm	z mm	az deg	el deg	Δ_x mm	Δ_y mm	Δ_z mm
4	-21440	5	11612	65539	849453	172	80	1	-3	1
4	-21440	5	11697	64998	865964	172	65	1	-4	3
4	-21440	5	12451	60251	881773	172	50	2	-4	3
4	-21440	5	13817	51622	895797	172	35	-4	1	3
4	-21440	5	15711	39699	907080	172	20	-7	9	7
4	-21440	6	12207	61829	833348	172	95	4	-2	-1
5	21440	5	-31409	58681	849421	172	80	4	-2	-3
5	21440	5	-31324	58149	865930	172	65	3	-3	-1
5	21440	5	-30570	53408	881740	172	50	1	-5	1
5	21440	5	-29201	44784	895768	172	35	-3	-3	3
5	21440	5	-27307	32864	907056	172	20	-8	1	8
5	21440	6	-30817	54968	833319	172	95	5	2	-7

Each line of the data table specifies the independent and dependent variables for an observation. The `retro` codes are arbitrary code numbers assigned to the targets, whose node IDs are shown in the `node` column; these small integer codes are used because the current version of Gaussfit does not operate correctly if arbitrary large integer values are used as subscripts. The Δ_x, Δ_y and Δ_z columns are the observed-minus-computed residuals for the observations with the parameter values which are tabulated below; the RMS of these residuals is displayed in Table 4:

Table 4: Sigma of the fit

cpsFit1Env.gf
σ mm
5.6

The LS fit used node coordinates and gravity deflections which were obtained from the FEM file for the targets by an ANSI-C program [KR88] which calls functions from the FEM software [Wel00] to load the specified FEM file and locate the coordinates and deflection values for the specified nodes. The node coordinates (`axis` = 0 is X, `axis` = 2 is Z) are in column `grid` of Table 5 below; the gravity deflections for $E = 90°$ and $E = 0°$ are in columns `ztrans` and `htrans`:

Table 5: Grid coordinates & FEM deflections

cpsFit1Param1					
retro	axis	nodeid	grid mm	ztrans mm	htrans mm
1	0	-20440	-21768	-2	7
1	1	-20440	-62927	-10	24
1	2	-20440	0	-113	47
4	0	-21440	-21768	-4	4
4	1	-21440	-60881	20	1
4	2	-21440	-16737	-110	42
2	0	20440	21768	2	-7
2	1	20440	-62927	-10	24
2	2	20440	0	-113	47

continued..

continued..

retro	axis	nodeid	grid mm	ztrans mm	htrans mm
5	0	21440	21768	4	-4
5	1	21440	-60881	20	1
5	2	21440	-16737	-110	42
3	0	31020	0	0	0
3	1	31020	-60881	24	3
3	2	31020	-16737	-118	43

This first LS fit solves for the offset vectors of these five targets relative to their nearby "elbow" nodes; these offsets are in the dgrid column of Table 6 below. Note that these dgrid values are added to the grid values at lines 108–110 of the model (Table 2 on page 5) to form the XYZ tipping coordinates of the targets. The formal errors of the LS solutions for these offsets are given in the $\sigma_{\mathtt{dgrid}}$ column:

Table 6: Adjusted coordinate offsets & deflections

cpsFit1Param2							
retro	axis	node	dgrid mm	dlock mm	dztrans mm	dhtrans mm	$\sigma_{\mathtt{dgrid}}$ mm
1	0	-20440	-406	0	0	0	3
1	1	-20440	31	0	0	0	2
1	2	-20440	89	0	0	0	2
4	0	-21440	6	0	0	0	3
4	1	-21440	6	0	0	0	2
4	2	-21440	-249	0	0	0	2
2	0	20440	443	0	0	0	3
2	1	20440	22	0	0	0	2
2	2	20440	61	0	0	0	2
5	0	21440	31	0	0	0	3
5	1	21440	24	0	0	0	2
5	2	21440	-274	0	0	0	2
3	0	31020	11	0	0	0	3
3	1	31020	2	0	0	0	2
3	2	31020	-264	0	0	0	2

Note in Table 6 above that the X offset of target -20440 on the left side at an upper corner of the elbow structure is about as much to the left of node -20440 as target +20440 on the right side is to the right of its node; each is $\approx$ 42 cm ($\approx$ 16.5 inch) from its node point, which is inside a welded joint structure connecting several large steel beams. The table shows that the Z offsets of targets $\pm$21440 at the lower corners of the elbow structure are both $\approx$ 26 cm ($\approx$ 10 inch); these retrospheres are almost directly below their nodes. Likewise, we see that retrosphere 31020 in the middle of the lower edge of the elbow is directly below its node by about the same amount.

As discussed earlier, I have adopted D. Parker's measurement of the height of the elevation axle; it is ez in Table 7 on the next page below. The LS fit solves for the azimuth zero point correction; it is azc in the table, with value -539 ± 10 arcsec (note the presence of $\sigma_{\mathtt{azc}}$ in the table). Recall that D. Parker measured -541 arcsec for azc; the agreement is effectively *exact*. Taken at face value, this agreement means that the LS fitting process is definitely correctly inferring the azimuth of the axle as the tipping structure moves in elevation:

Table 7: Position & orientation of azimuth & elevation axes

cpsFit1Param3												
rig deg	convang deg	eac arcsec	ex mm	ey mm	ez mm	azc arcsec	zvy arcsec	zvx arcsec	px mm	py mm	pz mm	σ_{azc} arcsec
50.8	0.717222	0	0	0	-44	-539	0	0	0	0	0	10

We have 40 observations in Table 3 on page 9; some of these are of the same target at the same elevation, and so are not truly independent pieces of data, but we will ignore this detail and will say that there are $40 \times 3 = 120$ data values to be fitted. We have 5 targets in Table 6 on the page before, with XYZ parameters for dgrid, or $5 \times 3 = 15$ parameters, plus azc in Table 7 for a total of 16. Therefore, the ratio of data values to parameters in this LS fit is more than 4×; the author's experience shows that 2× overdetermined is generally sufficient for robust LS solutions.

The parameter estimates produced by a LS fitting solution are generally correlated at some level. Table 8 below tabulates the largest correlation coefficients ρ_{ij} in this first LS solution; in particular note that azc is correlated with the X coordinates (axis=0) of the offset vectors to the targets. If we only had observations at high elevations these correlations would be near unity, and it would not be possible to determine the variables separately. However, when the GBT is at low elevations the elbow of the GBT feedarm is high in the air, nearly over the azimuth axle, and the variables become nearly uncorrelated; it is the existence of observations in Table 3 on page 9 with el values of 5° and 20° which enables us to get reasonable solutions for these correlated parameters:

Table 8: Significant parameter correlations

cpsFit1Results.out.corr cases with $\lvert\rho_{ij}\rvert > 0.50$		
P_i	P_j	ρ_{ij}
dgrid[1,0]	azc	0.808
dgrid[4,0]	azc	0.781
dgrid[5,0]	azc	0.753
dgrid[2,0]	azc	0.732
dgrid[3,0]	azc	0.712
dgrid[1,0]	dgrid[4,0]	0.631
dgrid[1,0]	dgrid[5,0]	0.608
dgrid[1,0]	dgrid[2,0]	0.591
dgrid[4,0]	dgrid[5,0]	0.587
dgrid[1,0]	dgrid[3,0]	0.576
dgrid[2,0]	dgrid[4,0]	0.571
dgrid[4,0]	dgrid[3,0]	0.556
dgrid[2,0]	dgrid[5,0]	0.551
dgrid[3,0]	dgrid[5,0]	0.536
dgrid[2,0]	dgrid[3,0]	0.521

On the basis of experience with a wide variety of LS problems, the author generally regards ρ values of 0.85 or larger as cause for concern, and values of 0.8 or less as acceptable; of course, $\rho \approx 0$ (orthogonality) is always best, but most non-trivial physical problems have some parameters with $\rho_{ij} > 0.5$.

3 Fit2 solution for feedarm tip position & FEM corrections

Now that we have determined the position and orientation of the elevation axle using the "elbow" targets, we can proceed to examine the data on the three feedarm tip targets, 41040L (see Figure 2 on page 4), 41040R (Figure 3 on page 19) and 41080 (Figure 1 on page 3). The model for this fit will lock the axle parameters and the target offset vectors determined in the first fit, but will solve for corrections to the FEM parameters. The differences between the first model (Table 2 on page 5) and the second model are shown in Table 9:

Table 9: Model changes for second fit to survey data

```
1c1
< /* cpsFit1Model.gf --- fit cardinal point survey data
---
> /* cpsFit2Model.gf --- fit cardinal point survey data
43c43
< parameter   azc;                  /* [arcsec] az zero point correction   */
---
> constant    azc;                  /* [arcsec] az zero point correction   */
52,53c52,53
< constant    dztrans[retro,axis]; /* [mm]  retro zenith  gravity delta   */
< constant    dhtrans[retro,axis]; /* [mm]  retro horizon gravity delta   */
---
> parameter   dztrans[retro,axis]; /* [mm]  retro zenith  gravity delta   */
> parameter   dhtrans[retro,axis]; /* [mm]  retro horizon gravity delta   */
```

Note that azc is a constant, a locked parameter, in the second model, but that dztrans and dhtrans are now declared as parameter. The data for the second fit, shown in Table 10, are the observations used in the first fit plus observations of the three feedarm tip targets:

Table 10: Survey data, with residuals from model fit

cpsFit2Data										
retro	node	run	x mm	y mm	z mm	az deg	el deg	Δ_x mm	Δ_y mm	Δ_z mm
1	-20440	1	12056	65376	850195	172	95	1	2	1
1	-20440	1	12168	64651	866621	172	80	-0	-1	3
1	-20440	1	12946	59751	882295	172	65	1	-2	2
1	-20440	1	14337	51004	896154	172	50	0	-6	5
1	-20440	1	16245	39013	907244	172	35	1	-4	5
1	-20440	1	18540	24593	914806	172	20	1	-1	1
1	-20440	1	21063	8732	918327	172	5	-1	3	0
1	-20440	2	18539	24593	914804	172	20	1	-1	-1
1	-20440	2	16241	39013	907239	172	35	-3	-4	-0
1	-20440	2	14337	51005	896153	172	50	0	-5	3
1	-20440	2	12947	59753	882292	172	65	1	-0	0
1	-20440	2	12166	64649	866618	172	80	-2	-3	-1
1	-20440	2	12055	65373	850194	172	95	-1	-0	-2
2	20440	3	-31789	58409	850160	172	95	1	1	-1
2	20440	3	-31676	57693	866594	172	80	-2	-1	5
2	20440	3	-30891	52799	882272	172	65	2	-2	3
2	20440	3	-29499	44056	896137	172	50	1	-3	3

continued..

continued..

retro	node	run	x mm	y mm	z mm	az deg	el deg	Δ_x mm	Δ_y mm	Δ_z mm
2	20440	3	-27590	32063	907234	172	35	-0	-3	3
2	20440	3	-25294	17638	914801	172	20	-1	-2	-0
2	20440	3	-22766	1772	918326	172	5	0	1	-0
2	20440	4	-31790	58407	850159	172	95	-0	-1	-2
3	-41040	1	-7840	69384	913819	172	95	3	1	3
3	-41040	1	-5092	52080	929901	172	80	-2	-5	0
3	-41040	1	-1775	31266	940881	172	65	0	-0	1
3	-41040	1	1875	8354	946014	172	50	0	-1	3
3	-41040	1	5612	-15074	944950	172	35	2	-2	1
3	-41040	1	9172	-37412	937778	172	20	0	0	0
3	-41040	1	12319	-57138	925003	172	5	0	0	1
3	-41040	2	9169	-37412	937776	172	20	-2	-0	-2
3	-41040	2	5607	-15072	944946	172	35	-2	-0	-3
3	-41040	2	1878	8358	946014	172	50	2	2	3
3	-41040	2	-1776	31270	940877	172	65	-1	3	-3
3	-41040	2	-5091	52087	929899	172	80	-1	1	-1
3	-41040	2	-7843	69383	913815	172	95	-1	0	-2
4	41040	3	-14049	68430	913816	172	95	1	-0	2
4	41040	3	-11292	51124	929906	172	80	4	-4	-1
4	41040	3	-7981	30302	940894	172	65	-2	1	-0
4	41040	3	-4329	7381	946031	172	50	-0	-1	2
4	41040	3	2966	-38397	937799	172	20	-0	3	1
4	41040	3	6113	-58135	925018	172	5	0	-1	-2
4	41040	4	-14052	68432	913812	172	95	-3	2	-2
5	41080	5	-12008	75551	913161	172	95	-1	2	1
5	41080	5	-9250	58189	931027	172	80	3	-2	-0
5	41080	5	-5858	36858	943710	172	65	-3	2	1
5	41080	5	-2049	13011	950344	172	50	1	-1	-0
5	41080	6	-12011	75566	913136	172	95	-0	-1	-1
6	31020	5	-9891	62122	849435	172	80	-0	1	0
6	31020	5	-9807	61586	865949	172	65	1	-3	2
6	31020	5	-9050	56841	881763	172	50	6	-6	1
6	31020	5	-7682	48210	895792	172	35	2	-5	0
6	31020	5	-5791	36286	907082	172	20	-3	-0	3
6	31020	5	-3496	21878	914846	172	5	1	1	-1
7	-21440	5	12205	61834	833363	172	95	0	-1	-2
7	-21440	5	11612	65539	849453	172	80	-2	0	2
7	-21440	5	11697	64998	865964	172	65	-1	-2	3
7	-21440	5	12451	60251	881773	172	50	2	-4	3
7	-21440	5	13817	51622	895797	172	35	-1	-3	1
7	-21440	5	15711	39699	907080	172	20	-0	1	0
7	-21440	6	12207	61829	833348	172	95	1	0	1
8	21440	5	-31409	58681	849421	172	80	-1	-2	1
8	21440	5	-31324	58149	865930	172	65	0	-3	1
8	21440	5	-30570	53408	881740	172	50	1	-5	1
8	21440	5	-29201	44784	895768	172	35	0	-4	-1
8	21440	5	-27307	32864	907056	172	20	-0	1	0
8	21440	6	-30817	54968	833319	172	95	0	1	-1

The model used in the second fit solves for the FEM correction parameters for the targets, which enables it to fit the observations much more closely, as shown in Table 11:

Table 11: Sigma of the fit

cpsFit2Env.gf
σ
mm
2.4

The node coordinates and FEM gravity displacements of the eight targets are tabulated in Table 12:

Table 12: Grid coordinates & FEM deflections

cpsFit2Param1					
retro	axis	nodeid	grid	ztrans	htrans
			mm	mm	mm
1	0	-20440	-21768	-2	7
1	1	-20440	-62927	-10	24
1	2	-20440	0	-113	47
7	0	-21440	-21768	-4	4
7	1	-21440	-60881	20	1
7	2	-21440	-16737	-110	42
3	0	-41040	-2694	0	-0
3	1	-41040	-64011	-153	345
3	2	-41040	64369	-125	66
2	0	20440	21768	2	-7
2	1	20440	-62927	-10	24
2	2	20440	0	-113	47
8	0	21440	21768	4	-4
8	1	21440	-60881	20	1
8	2	21440	-16737	-110	42
6	0	31020	0	0	0
6	1	31020	-60881	24	3
6	2	31020	-16737	-118	43
4	0	41040	2694	-0	0
4	1	41040	-64011	-153	345
4	2	41040	64369	-125	66
5	0	41080	0	0	0
5	1	41080	-70803	-153	346
5	2	41080	64369	-139	108

The geometric parameters of our model are all held constant at the values used or determined in the first fit:

Table 13: Position & orientation of azimuth & elevation axes

cpsFit2Param3											
rig	convang	eac	ex	ey	ez	azc	zvy	zvx	px	py	pz
deg	deg	arcsec	mm	mm	mm	arcsec	arcsec	arcsec	mm	mm	mm
50.8	0.717222	0	0	0	-44	-539	0	0	0	0	0

The target offset vectors from the node coordinates are in the dgrid column of Table 14. These values should be locked for the elbow targets which were fitted in the first LS solution; this is accomplished by a program which extracts the dgrid values from Table 6 on page 11 and places them in the dlock column of Table 14. The code in lines 76–81 of the model (Table 2 on page 5) finds the nonzero dlock values and uses them in the Gaussfit function call exportconstraint() to lock these parameters; note that $\sigma_{\mathtt{dgrid}} = 0$ for these parameters.

Table 14: Adjusted coordinate offsets & deflections

cpsFit2Param2									
retro	axis	node	dgrid mm	dlock mm	dztrans mm	dhtrans mm	$\sigma_{\mathtt{dgrid}}$ mm	$\sigma_{\mathtt{dhtrans}}$ mm	$\sigma_{\mathtt{dztrans}}$ mm
1	0	-20440	-406	-406	5	-1	0	3	4
1	1	-20440	31	31	23	-9	0	3	4
1	2	-20440	89	89	21	6	0	3	4
7	0	-21440	6	6	-13	-0	0	4	7
7	1	-21440	6	6	23	3	0	4	7
7	2	-21440	-249	-249	21	9	0	4	7
3	0	-41040	-470	0	33	0	1	4	5
3	1	-41040	-171	0	41	-56	1	4	5
3	2	-41040	-265	0	49	16	1	4	5
2	0	20440	443	443	2	-1	0	3	4
2	1	20440	22	22	14	-5	0	3	4
2	2	20440	61	61	6	9	0	3	4
8	0	21440	31	31	-17	2	0	4	7
8	1	21440	24	24	22	7	0	4	7
8	2	21440	-274	-274	3	9	0	4	7
6	0	31020	11	11	-3	8	0	7	6
6	1	31020	2	2	4	-11	0	7	6
6	2	31020	-264	-264	14	7	0	7	6
4	0	41040	422	0	25	-3	2	5	6
4	1	41040	-193	0	43	-38	2	5	6
4	2	41040	-260	0	46	23	2	5	6
5	0	41080	-19	0	130	32	2	10	32
5	1	41080	-159	0	31	-66	2	10	32
5	2	41080	-299	0	105	32	2	10	32

As we saw with the elbow node offsets in Table 6 on page 11, the offset vectors dgrid for the three feedarm tip nodes in Table 14 are plausible. The two ±41040 targets are about 44 cm (17 inches) outward in X from their nodes, about 18 cm backward (-Y, away from the main mirror) and about 26 cm downward (-Z, toward the elbow). The 41080 target offset is similar: it is on the plane of symmetry ($X = 0$), about 16 cm backward and about 30 cm downward.

The dztrans and dhtrans columns of Table 14 are the corrections to the FEM gravity deflections which the LS fit infers from the deviations of the arcs from circularity after the predicted deflections are compensated. These corrections are about 20 mm or less for the five elbow targets; the formal errors for these parameters are about 6 mm, which is large enough to raise questions about statistical significance, especially considering the correlations discussed below. The author does not think it would be prudent to conclude that these data imply that the *symmetric* Model 97 is not predicting the box structure properly.

The two ±41040 targets have larger FEM corrections, and do appear to be statistically significant; they will be discussed in Section 3.1 on page 18.

We have 65 observations in Table 10 on page 13, so there are $65 \times 3 = 195$ data values to be fitted. We have 8 targets in Table 14 on the facing page, with XYZ parameters for `dgrid`, `dhtrans` and `dztrans`, or $8 \times 3 \times 3 = 72$ parameters, but the `dgrid` values for 5 targets are locked, so the number of active parameters is $72 - 5 \times 3 = 57$. Therefore, the ratio of data values to parameters in this LS fit is more than $3\times$.

However, target 41080 was not observed at low elevations, and therefore has large formal errors on its corrections. Because it was inadequately observed, its corrections also exhibit very high correlations:

Table 15: Significant parameter correlations

`cpsFit2Results.out.corr` cases with $\|\rho_{ij}\| > 0.50$		
P_i	P_j	ρ_{ij}
dhtrans[5,1]	dztrans[5,1]	0.925
dhtrans[5,2]	dztrans[5,2]	0.925
dhtrans[5,0]	dztrans[5,0]	0.925
dhtrans[4,0]	dztrans[4,0]	0.903
dhtrans[4,2]	dztrans[4,2]	0.903
dhtrans[4,1]	dztrans[4,1]	0.903
dhtrans[3,0]	dztrans[3,0]	0.894
dhtrans[3,2]	dztrans[3,2]	0.894
dhtrans[3,1]	dztrans[3,1]	0.894
dztrans[6,1]	dhtrans[6,1]	0.869
dztrans[6,2]	dhtrans[6,2]	0.869
dztrans[6,0]	dhtrans[6,0]	0.869
dhtrans[7,1]	dztrans[7,1]	0.827
dhtrans[7,2]	dztrans[7,2]	0.827
dhtrans[7,0]	dztrans[7,0]	0.827
dztrans[8,2]	dhtrans[8,2]	0.822
dhtrans[8,1]	dztrans[8,1]	0.822
dhtrans[8,0]	dztrans[8,0]	0.822
dgrid[4,2]	dhtrans[4,2]	0.818
dgrid[4,1]	dhtrans[4,1]	0.818
dgrid[4,0]	dhtrans[4,0]	0.818
dhtrans[1,2]	dztrans[1,2]	0.777
dhtrans[1,0]	dztrans[1,0]	0.777
dhtrans[1,1]	dztrans[1,1]	0.777
dgrid[4,1]	dztrans[4,1]	0.775
dgrid[4,2]	dztrans[4,2]	0.775
dgrid[4,0]	dztrans[4,0]	0.775
dhtrans[2,0]	dztrans[2,0]	0.747
dhtrans[2,1]	dztrans[2,1]	0.747
dhtrans[2,2]	dztrans[2,2]	0.747
dgrid[3,1]	dhtrans[3,1]	0.731
dgrid[3,2]	dhtrans[3,2]	0.731
dgrid[3,0]	dhtrans[3,0]	0.731
dgrid[3,1]	dztrans[3,1]	0.721
dgrid[3,2]	dztrans[3,2]	0.721
dgrid[3,0]	dztrans[3,0]	0.721
dgrid[5,1]	dztrans[5,1]	-0.508
dgrid[5,0]	dztrans[5,0]	-0.508
dgrid[5,2]	dztrans[5,2]	-0.508

Note that the FEM corrections for each target appear to be rather strongly correlated with the target's offset vector. This indicates that the choice of variables used here is suboptimal; we will discuss this further in Section 3.2 on page 22.

3.1 Properties of the feedarm tip trajectory

The coordinates of nodes near the three feedarm tip targets and their gravity deflections as predicted by Model 97s are tabulated in Table 16; note the mirror symmetry patterns in both the coordinates and the deflections.

Table 16: Model 97s node coordinates and gravity deflections

nodeid	gridx	gridy	gridz	dx_zen	dy_zen	dz_zen	dx_hor	dy_hor	dz_hor
		mm			mm			mm	
-41040	-2694	-64011	64369	0.1	-152.7	-124.9	-0.4	344.7	66.2
41040	2694	-64011	64369	-0.1	-152.7	-124.9	0.4	344.7	66.2
41080	0	-70803	64369	0.0	-152.9	-139.4	0.0	346.1	108.0

The observed node-to-target offset vectors and the gravity deflection corrections for the three targets are tabulated in Table 17. Table 14 on page 16, in which the same numbers appear, shows that the trajectory of the 41080 target is poorly determined, with large formal error, due to no observations at low elevations (see Table 10 on page 13); therefore this target will not be discussed further here. Instead, the feedarm tip trajectory will be summarized by summing the the trajectories of the two 41040 targets as specified in Table 17 to produce the trajectory of the bisecting point (the two targets are identified in Figure 3 on the next page). Unlike the Model 97s predicted trajectories, the two observed trajectories display an asymmetry; this can be summarized as an average deflection out of the plane of symmetry plus a rotation of the tip which can be computed by differencing the trajectories.

Table 17: Observed offsets & corrections to gravity deflections

nodeid	dgridx	dgridy	dgridz	ddx_zen	ddy_zen	ddz_zen	ddx_hor	ddy_hor	ddz_hor
		mm			mm			mm	
-41040	-470	-171	-265	33.3	40.8	48.6	0.3	-55.9	16.0
41040	422	-193	-260	25.1	42.8	46.5	-3.2	-38.0	23.3
41080	-19	-159	-299	130.3	31.0	104.7	31.6	-66.5	32.4

Table 18 on the facing page shows the predicted (Model 97s) trajectory of the bisecting point as (x_p,y_p,z_p). The values tabulated for the rigging angle are the tipping coordinates of the bisector of the line between the nodes. The main body of these columns tabulates the trajectory of the bisector relative to the position at the rigging angle. The values tabulated for $E = 0$ are the total travel of the trajectory over $5° < E < 95°$. The table also shows the observed trajectory of the bisecting point between the two trajectories of the targets near the nodes as (x_o,y_o,z_o). Note the 28 mm motion in x_o; this is due to the elevator asymmetry of the feedarm mass distribution, and was not predicted by the symmetric FEM ($x_p = 0$). The observed distance between the targets r_o is tabulated as a check (it should be essentially constant); the 5 mm variation over $5° \mapsto 95°$ is certainly acceptable considering the accuracy of the Topcon data. The twist about Z_{tipping} of the 6.3 meter line connecting the nodes is tabulated as θ_o; this is another observed asymmetry of the GBT feedarm deflections, and it will be discussed further on page 21.

Figure 3: GBT feedarm tip viewed from the front side, with two targets marked

Note that the observed total gravitational deflection of the GBT tipping structure for $5° < E < 95°$ in the Y tipping coordinate is only 83 percent ($\frac{423}{512}$) of the Model 97s prediction; in Z tipping it is 88 percent ($\frac{163}{185}$) of the predicted travel. I.e., the feedarm is stiffer in Y_{tipping} and Z_{tipping} than was expected.

Table 18: ±41040-bisector position & rotation

E	x_p	y_p	z_p	x_o	y_o	z_o	θ_p	θ_o	r_p	r_o
deg	mm (predicted Model 97)			mm (observed by [PS00])			mr	mr	mm	mm
50.8	0	-64011	64369	-24	-64193	64106	0.0	-3.5	5388	6280
5.0	0	231	110	-21	185	84	0.0	0.8	0	5
10.0	0	213	98	-18	172	77	0.0	0.8	0	4
15.0	0	194	87	-16	157	69	0.0	0.8	0	3
20.0	0	172	74	-13	140	60	0.0	0.7	0	3
25.0	0	148	62	-11	121	51	0.0	0.7	0	2
30.0	0	123	50	-8	100	41	0.0	0.6	0	2
35.0	0	95	38	-6	78	32	0.0	0.5	0	1
40.0	0	66	25	-4	55	22	0.0	0.3	0	1
45.0	0	36	13	-2	30	12	0.0	0.2	0	0
50.0	0	5	2	-0	4	2	0.0	0.0	0	0
55.0	0	-27	-9	1	-22	-8	0.0	-0.2	-0	-0
60.0	0	-59	-20	3	-49	-18	0.0	-0.3	-0	-0
65.0	0	-92	-30	4	-77	-28	0.0	-0.6	-0	-1
70.0	0	-125	-40	5	-105	-38	0.0	-0.8	-0	-1
75.0	0	-158	-49	6	-132	-47	0.0	-1.0	-0	-1
80.0	0	-190	-57	7	-160	-56	0.0	-1.2	-0	-0
85.0	0	-222	-64	7	-187	-64	0.0	-1.5	-0	-0
90.0	0	-252	-70	7	-213	-72	0.0	-1.7	-1	-0
95.0	0	-282	-75	8	-239	-79	0.0	-2.0	-1	0
0.0	0	-512	-185	28	-423	-163	0.0	-2.8	-1	-5

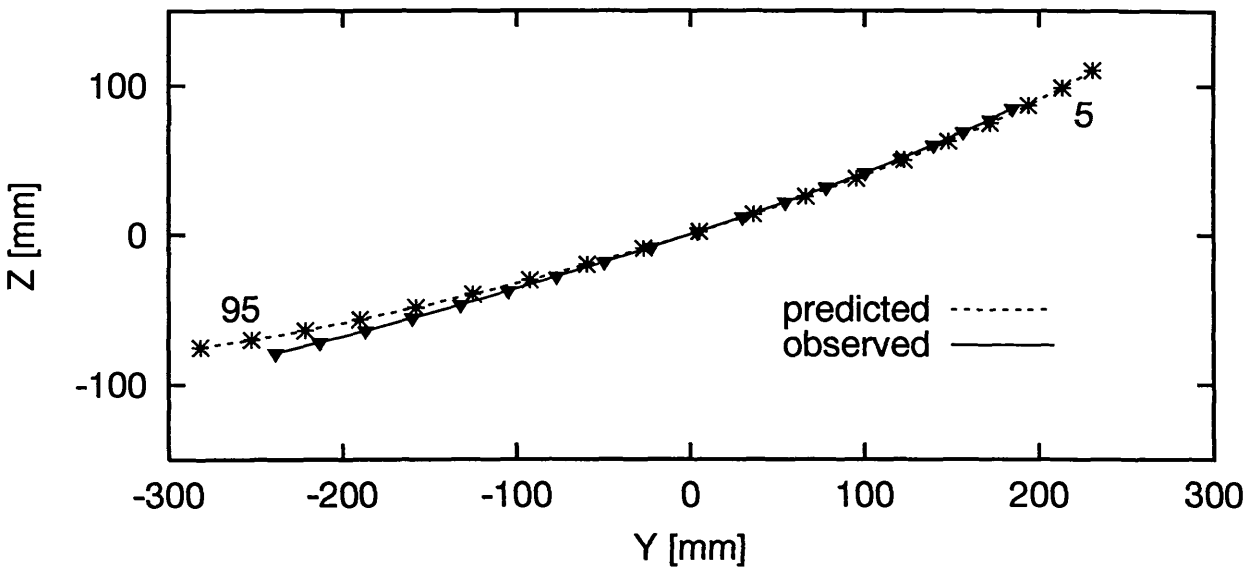

Figure 4: Trajectories of the tip of the feedarm

Figure 4 shows that not only does the observed total travel of the feed arm tip trajectory differ from the FEM prediction, but the shape also differs. The author is unable to say anything about this discrepancy.

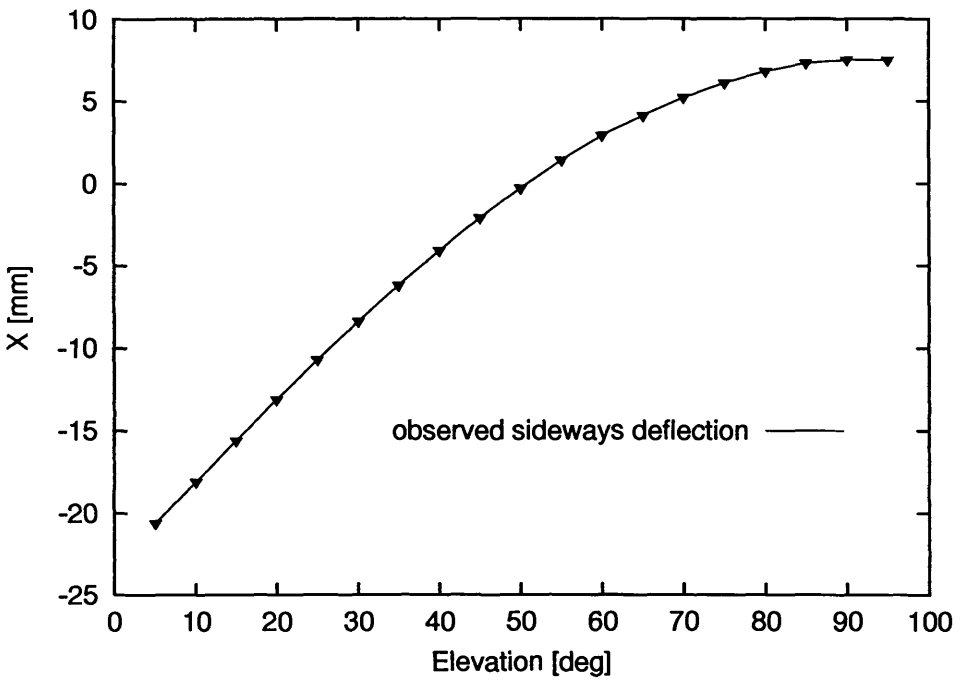

Figure 5: Sideways deflection of the tip of the feedarm

The observed feedarm tip trajectory (Figure 5,Table 18 on the preceding page) has x_o going negative at low elevations; this is intuitively plausible, because at high elevations the mass asymmetry twists the horizontal feedarm and moves the tip to the right (positive), and at low elevations this loading is removed and the arm

springs back to the left. The total motion over 5° ↦ 95° is +28 mm. Both Model 95b and Model 97s are symmetric FEMs (mirror symmetry about the Y-Z plane), so they don't predict this X motion. In Loral Tech Memo 46 [Zai92], an included memorandum by D.L. Enterline says that the motion of the subreflector in X (Z in subreflector coordinates) needs to be ±0.83 inch, or 1.66 inch=42 mm total. It was this report which set the specifications for Z-actuator travel in the subreflector actuator system. Presumably Loral used a structural model which included the asymmetric mass distribution in order to predict this number. If this predicted subreflector Z motion requirement is the same quantity as the x_o feedarm motion we are observing, then we are observing only about 64 percent ($\frac{28}{42}$) of the predicted X deflection. If so, then this is another discrepancy between observations and predictions.

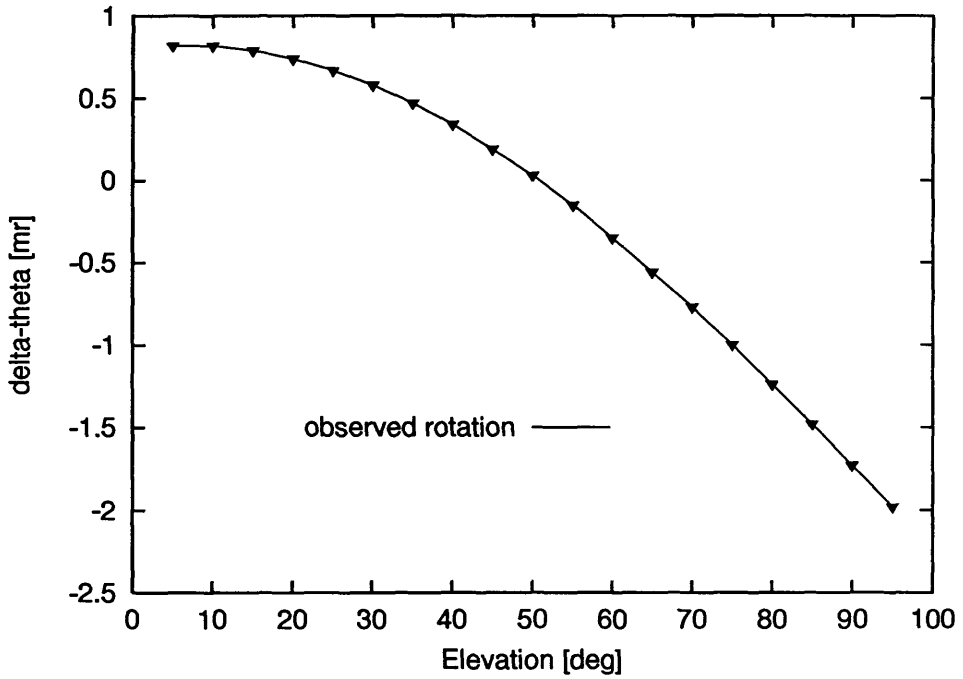

Figure 6: Rotation of the tip of the feedarm

The two ±41040 targets are 6.3 meter (r_o) apart; the geodetic total station should be capable of measuring the angular orientation of the line connecting them with a precision of better than one milliradian. The observed rotation is -2.8 mr over $5° < E < 95°$. This rotation is expected because of the asymmetric mass distribution: at low elevations the excess mass on the right-hand side should cause the feedarm to twist clockwise (as seen when looking parallel to the arm in the $+Z_{\text{tipping}}$ direction). This should cause Y_{tipping} on the right to increase (toward the ground at low elevations) more than on the left. The formula used for the angle of the ±41404 line is

$$\theta = \frac{Y_{+41404} - Y_{-41404}}{r_o},$$

so increasing Y more on the right-hand side should cause θ to increase at low elevations, which is what we observe in Figure 6. This rotation will be compensated in the Gregorian focus tracking algorithm [Wel98b, this rotation is `subr_center.at_elev[2]` at Step 14 on p.10] if it is in the FEM, either because the FEM is asymmetric or because we have augmented it with empirical corrections such as those in Table 18 on page 19.

An important conclusion of this work is that the observed total travel of the feedarm tip is well within the subreflector actuator capabilities which were specified and built on the basis of FEM analysis, because the feedarm appears to be stiffer than was expected.

3.2 Planes and parameters: conjectures about fitting trajectories

Fred Schwab [private communication], in an independent analysis of the same Topcon dataset, used Singular Vector Decomposition [SVD] to fit to the XYZ points of the trajectory arcs of the target retrospheres. SVD is an especially efficient and elegant technique for fitting planes to points in space. It was natural to assume that a plane fitted to the trajectory arc of node 31020, which lies in the plane of symmetry (Figure 1 on page 3), would indicate the azimuth zero point (azc) neatly, whereas the arcs of other targets might depart from planes somewhat due to gravitational deflections. However, Schwab's SVD solution displayed the astonishing property that *all of the target arcs* (not just 31020) lie in *planes* with remarkable precision: the RMS residuals normal to the planes are of order 1.5 millimeters! In response to a query on this matter, Lee King [private communication] has asserted that this behavior is indeed a property of the arcs of all nodes in the tipping structure, that it is a consequence of the mathematics and physics. The planes are not all normal to the elevation axle, of course.

This mathematical fact could potentially help in determining empirical FEM corrections, such as those in Table 18 on page 19. This would be because a proper formulation of the arc trajectories in planes would be a more orthogonal representation of the problem, which should produce lower correlations than those in Table 15 on page 17. Also, the author suspects that such a representation might need only eight parameters per node[7], rather than the nine parameters[8] used in Table 18 on page 19; this would improve the formal errors of the fit somewhat.

[7] XYZ at rigging angle, two plane tilts, radius, eccentricity and angle of major axis (if the arcs are ellipses)
[8] XYZ at rigging angle, delta-XYZ at zenith, delta-XYZ at horizon

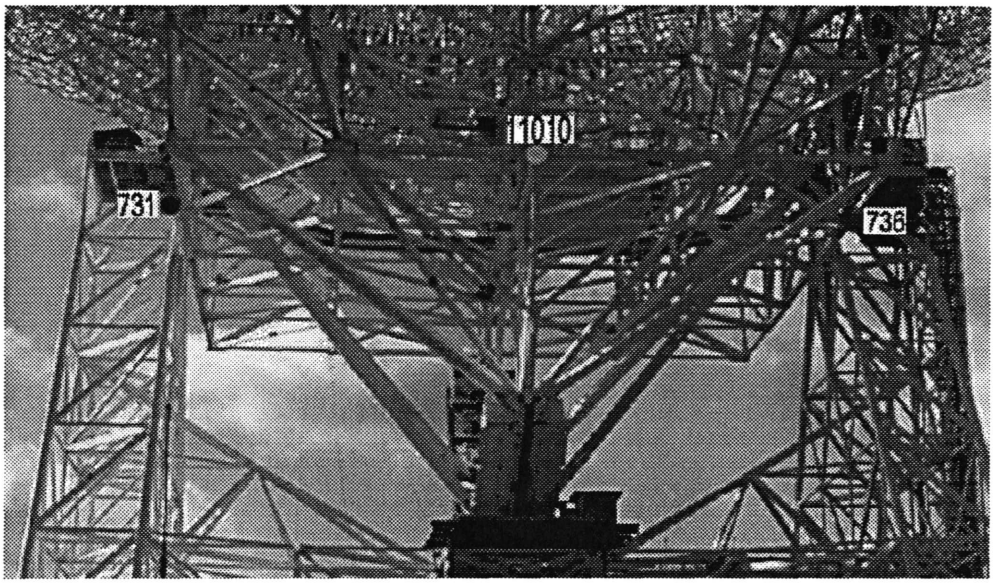

Figure 7: GBT alidade and elevation axle bearings, viewed from the feedarm (back) side, with targets marked

4 Fit3 solution for azimuth axis lateral offset

The locations of the special retrosphere targets 731 and 736 are shown in Figure 7, mounted directly below the elevation axle bearing housings; 736 is on the right-hand side (the $+X_{\text{alidade}}$ side) of the alidade structure. These targets are "special" because they consist of two retrospheres, one facing forward (toward $+Y_{\text{alidade}}$) and the other facing backward, in a special mounting which assures that their reflection points have a known spacing [She00]. They have been mounted such that the line connecting their reflection points is parallel to the elevation axis with high precision; as we will see, the line is also very nearly directly under the the elevation axis. The purpose of these targets is to measure changes in the azimuth zero point (twist of the alidade) and the tilt of the elevation axle (change of the horizontal collimation angle) using the ring-of-fire laser rangefinders [Gol97].

The cardinal point survey dataset contains a modest number of measures of these targets, at four azimuths. It is feasible to try a solution for the offset vectors of the four target retrospheres plus the X and Y offsets of the azimuth axis relative to the origin of the ring-of-fire pier coordinates. In principle an extensive dataset on these targets in multiple azimuths uniformly distributed should support a solution for the zenith vector of the azimuth track, as was noted in a footnote on page 5. It should also permit estimation of the higher-order terms of the azimuth track.

The Gaussfit model for this alidade solution is still the one shown in Table 2 on page 5, but with the changes shown in Table 19 on the following page: `azc` is locked and `px` and `py` are activated as parameters. The latter are the X and Y offsets of the pintle bearing (i.e. the azimuth axis), which is the nominal origin of the coordinates of the ring-of-fire piers. A parameter file supplied to Gaussfit contains a value for the `csystem` code for each target; the code is 1 for tipping targets and 0 for alidade targets. This code is tested at line 112 of Table 2 on page 5 to control whether the translations and rotations appropriate for tipping targets are applied (lines 113–138); for alidade targets an `else` clause at lines 141–147 is executed. In the case of this fit it will add the static deflections predicted by the alidade FEM. The alidade-related transformations appropriate for all nodes are applied at lines 150–165.

Table 19: Model changes for fit to alidade retroreflector data

```
1c1
< /* cpsFit1Model.gf --- fit cardinal point survey data
---
> /* cpsFit3Model.gf --- fit cardinal point survey data
43c43
< parameter   azc;                /* [arcsec] az zero point correction   */
---
> constant    azc;                /* [arcsec] az zero point correction   */
46,47c46,47
< constant    px;                 /* [mm]  X coord of pintle bearing     */
< constant    py;                 /* [mm]  Y coord of pintle bearing     */
---
> parameter   px;                 /* [mm]  X coord of pintle bearing     */
> parameter   py;                 /* [mm]  Y coord of pintle bearing     */
```

The available data are shown in Table 20.

Table 20: Survey data, with residuals from model fit

cpsFit3Data										
retro	node	run	x mm	y mm	z mm	az deg	el deg	Δ_x mm	Δ_y mm	Δ_z mm
1	731	7	-8169	22152	851948	71	90	1	-1	9
1	731	8	-23006	5307	851939	14	90	4	4	-0
2	-731	9	-6888	22254	851939	74	90	-2	2	0
2	-731	10	-6602	-22348	851940	287	90	1	-7	1
2	-731	5	23004	3643	851937	172	90	-2	1	-2
2	-731	5	23003	3639	851932	172	90	-4	-3	-6
2	-731	5	23007	3644	851938	172	90	1	2	-1
3	736	7	8190	-22169	851954	71	90	4	-1	10
3	736	8	23033	-5296	851938	14	90	6	1	-6
4	-736	9	6901	-22265	851944	74	90	0	4	1
4	-736	10	6590	22349	851938	287	90	-3	-9	-6
4	-736	5	-23024	-3660	851943	172	90	0	1	-1
4	-736	5	-23027	-3659	851944	172	90	-2	2	0
4	-736	5	-23027	-3660	851944	172	90	-2	1	1
4	-736	5	-23027	-3659	851944	172	90	-2	2	1

The model fits the data with fair precision:

Table 21: Sigma of the fit

cpsFit3Env.gf
σ mm
4.1

The alidade coordinates and static gravity deflection (due to the weight of the 5000-ton tipping structure on the elevation bearings) of the two alidade nodes are shown in Table 22.[9]

Table 22: Grid coordinates & FEM deflections

cpsFit3Param1					
retro	axis	nodeid	grid mm	ztrans mm	htrans mm
2	0	-731	-22631	2	0
2	1	-731	0	0	0
2	2	-731	48260	-24	0
4	0	-736	22631	-2	0
4	1	-736	0	0	0
4	2	-736	48260	-24	0
1	0	731	-22631	2	0
1	1	731	0	0	0
1	2	731	48260	-24	0
3	0	736	22631	-2	0
3	1	736	0	0	0
3	2	736	48260	-24	0

The offsets to the four target retrospheres are estimated with formal errors of order 1-2 millimeters:

Table 23: Adjusted coordinate offsets & deflections

cpsFit3Param2							
retro	axis	node	dgrid mm	dlock mm	dztrans mm	dhtrans mm	σ_{dgrid} mm
2	0	-731	-666	0	0	0	2
2	1	-731	17	0	0	0	2
2	2	-731	-3733	0	0	0	2
4	0	-736	683	0	0	0	1
4	1	-736	-4	0	0	0	1
4	2	-736	-3728	0	0	0	1
1	0	731	-983	0	0	0	2
1	1	731	17	0	0	0	2
1	2	731	-3733	0	0	0	2
3	0	736	1001	0	0	0	1
3	1	736	-4	0	0	0	1
3	2	736	-3728	0	0	0	1

There is a detail of the above offsets which is not obvious: they are two pairs of offsets whose X_{alidade} differences are constrained to laboratory calibration values [She00]. The constraint is accomplished by code in the model, at lines 84–98 of Table 2 on page 5. The zag flag which activates this constraint is supplied to Gaussfit in a parameter file, along with the retro codes for the four retrospheres, as shown in Table 24 on the next page. Note that the $\Delta Y_{\text{alidade}}$ (dgrid) offset values above are only a few millimeters (the targets are almost directly under the elevation axis).

[9]The alidade FEM is not symmetric; node 736 is on the right and 731 is on the left. In this third LS fit the targets are designated as ±731 and ±736, where the minus cases are not on the left but rather are the two retrospheres which look backward.

Table 24: ZAG flag and 'retro' codes

cpsFit3Param5				
zag	r731p	r731d	r736p	r736d
1	2	1	4	3

The final result of this third LS fit is the pintle offsets:

Table 25: Position & orientation of azimuth & elevation axes

cpsFit3Param3													
rig deg	convang deg	eac arcsec	ex mm	ey mm	ez mm	azc arcsec	zvy arcsec	zvx arcsec	px mm	py mm	pz mm	σ_{px} mm	σ_{py} mm
50.8	0.717222	0	0	0	-44	-541	0	0	-1	-2	0	1	1

The values $(\mathtt{px}, \mathtt{py}) = (-1 \pm 1, -2 \pm 1)$ are effectively *zero.*

There are no parameter correlations greater than 0.5 in this LS fit.

References

[Con92] J. J. Condon. GBT pointing equations. GBT Memo 75, National Radio Astronomy Observatory, 1992. Recommends that the GBT pointing coefficients be implemented as a 2D Fourier series.

[Gol96] M. A. Goldman. Ball retroreflector optics. GBT Memo 148, NRAO, March 1996. "..design and optical properties of ball retroreflectors are discussed. Ray tracing computations are given for.. reflectors to be used at the GBT.." (note that an erratum to p.6 was issued).

[Gol97] M. A. Goldman. Laser distance measurements to the elevation bearing support weldments. GBT Memo 164, National Radio Astronomy Observatory, March 1997. "..for any alidade azimuth, at least two ranging lines of sight are available on the right side of the alidade and two or more on the left side, to the bottom surface of each weldment.. the horizontal angle of the line between the [bearings] could be measured withing 1 arcsecond, and the vertical tilt of this line to 2 arcseconds.. ball retroreflectors.. would have to be viewed near the limits of their response range to return signal to both right and left side rangefinders..".

[JFMM88] William H. Jefferys, Michael J. Fitzpatrick, Barbara E. McArthur, and James E. McCartney. *User's Manual—GaussFit: A system for least squares and robust estimation.* The University of Texas at Austin, 1.0-12/2/88 edition, December 1988. Gaussfit is a program which supports a full-featured programming language in which models can be built to solve generalized least squares (both linear and nonlinear) and robust estimation problems. Derivatives are computed analytically, linear constraints and orthogonal distance regression are supported and errors in independent variables and correlated observations are handled correctly. See also `ftp://clyde.as.utexas.edu/pub/gaussfit/` and `http://clyde.as.utexas.edu/Gaussfit.html`.

[Kin96] Lee King. Cardinal points on feedarm and box/wheel structures. Email to D.Parker, D.Hogg, D.Wells, F.Schwab, R.Lacasse, D.Seaman, S.Smith, R.Norrod and R.Hall, 4 April 1996. This memo lists the node-IDs or coordinates of 14 points on the secondary optics, 8 near the elevation bearings, 20 on the box/wheel and horizontal feedarm and 12 on the back of the reflector backup structure. These "cardinal points" are recommended locations for retroreflector prisms for monitoring structural deflections.

[KR88] Brian W. Kernighan and Dennis M. Ritchie. *The C programming language.* Prentice Hall, Englewood Cliffs, New Jersey, second edition, 1988. ISBN=0-13110362-8 (paper), first edition was published in 1978.

[Par00] David H. Parker. "Azimuth encoder error and elevation axis height". Private Email 2000-10-03 from Dave Parker to 10 NRAO addresses, October 2000. "..results of the 9/28/00 survey of the GBT azimuth.. the indicated [azimuth] is 000-08-55 too much .. On 9/26, insulation was removed.. decrease.. indicated azimuth.. about 000-00-06 .. surveyed elevation of the elevation bearings is 855.654 meters and the GBT track is 807.438 meters, or a differential height of 48.216 m (1898.27 in) ..".

[PS00] David H. Parker and John Shelton. "GBT Survey Data". Private Email 2000-09-12 from John Shelton to Don Wells and Fred Schwab, September 2000. The message contained a table of 131 observations of XYZ coordinates of GBT targets made with the Topcon total station.

[She00] John Shelton. "ZAG736 and ZAG731". private Email 2000-10-10 from John Shelton to D. Wells, October 2000. "The distance between [elevation bearing retrospheres] ZAG731D and ZAG731P is 12.501 inches, .. between ZAG736D and ZAG736P is 12.505 inches".

[WCS96] Larry Wall, Tom Christianson, and Randal L. Schwartz. *Programming Perl.* O'Reilly & Associates, Sebastopol, CA, second edition, 1996. QA76.73.P47W34, ISBN 1-56592-149-6.

[Wel98a] Don Wells. The Condon Series pointing model in C. GBT Memo 173, NRAO, January 1998. An implementation in the C language of Condon's Fourier Series for the "traditional" telescope pointing model is presented. The interpretation of the terms is discussed, a fit of the pointing model to the GBT structural model is presented, and the potential for determination of some of the terms of the model by metrology is reviewed.

[Wel98b] Don Wells. GBT Gregorian focus tracking in C. GBT Memo 183, NRAO, June 1998. The GBT Gregorian subreflector, an off-axis portion of an ellipsoid, plus the feedroom with the feedhorn move relative to the prime focal point of the main paraboloidal mirror. The subreflector must be maneuvered relative to the prime focal point and the feedhorn to maintain nearly stigmatic imaging (maximum gain, minimum sidelobes). An algorithm is described which computes the required actuator motions as a function of elevation. Raytracing analysis shows that GBT wavefronts produced by this optical prescription exhibit *no* focus error, spherical abberation or coma; their only abberation is astigmatism, with amplitude 0.4 mm for $E = 0°$ and $E = 90°$.

[Wel00] Don Wells. New GBT structural model files and related functions in C. GBT Memo 20x, NRAO, November? (to be published) 2000. This report, which supercedes [WK95], documents a new implementation of the GBT finite-element models and related software, which now supports networked distribution and installation of revised models without recompilation of code. The revised implementation includes new versions of the BFP and focus tracking functions, and it includes corrections for thermal expansion. The new model files can contain eigenvectors and static force models, in addition to gravity models. See
`ftp://fits.cv.nrao.edu/pub/gbt_dwells_doc.tar.gz`
for the current revision of this memo.

[WK95] Don Wells and Lee King. The GBT Tipping-Structure Model in C. GBT Memo 124, NRAO, March 1995. Abstract: The finite element model of the GBT tipping structure has been translated into executable code expressed in the C language, so that it can be used by the control software modules for the pointing, focus-tracking, quadrant detector, active-surface and laser-rangefinder subsystems of the GBT. We give a description of this C-code version of the tipping structure model and two examples of its application to practical problems. See `ftp://fits.cv.nrao.edu/pub/gbt_dwells_doc.tar.gz` for the current revision of this memo (124.3 as of 1997-06-23; superceded by [Wel00]).

[Zai92] J. Zaine. Mechanical analysis S/R positioner. Loral GBT Technical Memo 46, Loral Western Development Labs, October 1992. This comprehensive report discusses operational, peak operational and survival loadings, required motor torques, lost motion (backlash) of the U-joints and possible structural interference and U-joint angle problems of the subreflector actuators. Portions of Loral Interoffice Memorandum 3WL110-DLE-107, by D. L. Enterline and titled "NRAO 100m GBT Prime Focus Feed & Subreflector Positioner Gravity Correction Travel Requirements", are included in Appendix A (pp.A1-A13). The asymmetric structural model which was used enabled calculation of the required out-of-plane Z_s translation ± 0.83in.